

Joint Concept Matching-Space Projection Learning for Zero-Shot Recognition

Wen Tang, Ashkan Panahi, and Hamid Krim

Department of Electrical and Computer Engineering

North Carolina State University, Raleigh, NC 27606

E-mail: {wtang6, apanahi, ahk}@ncsu.edu

Abstract—Zero-shot learning (ZSL) has been widely researched and achieved a great success in machine learning, which aims to recognize unseen object classes by only training on seen object classes. Most existing ZSL methods are typically to learn a projection function between visual feature space and semantic space and mainly suffer a projection domain shift problem, as there is often a large domain gap between seen and unseen classes. In this paper, we proposed a novel inductive ZSL model based on project both visual and semantic features into a common distinct latent space with class-specific knowledge and reconstruct both visual and semantic features by such a distinct common space to narrow the domain shift gap. We show that all these constraints of the latent space, class-specific knowledge, reconstruction of features and their combinations enhance the robustness against the projection domain shift problem and improve the generalization ability to unseen object classes. Comprehensive experiments on four benchmark datasets demonstrate that our proposed method is superior than state-of-the-art algorithms.

Index Terms—Common Distinct Latent Space, Class-specific Information, Reconstruction of Features, Inductive Zero-shot Learning.

1 INTRODUCTION

IN recent years, object recognition has been remarkably improved even on large-scale recognition problems, such as the ImageNet ILSVRC challenge [1]. The latest deep neural networks (DNN) architectures [2], [3], [4], [5], [6] reportedly achieve a super-human performance on the ILSVRC 1K recognition task. In spite of the existing successes, most techniques rely on the supervised training of DNNs to obtain visual representations of per category that supplied with abundant labeled training examples. In practice, however, the number of objects of different categories is not predetermined and often follows a long-tail distribution. Except for popular categories which have a large amount of training samples, most categories may have only few or no training samples. As a result, the capability of up-to-date DNN models in recognizing those scare objects is highly limited. Additionally, it is intractable to manually collect and annotate the training samples for each object category. Simply for animal recognition problem, as example, there are about 8.7 million different animal species on earth to learn. Zero short learning (ZSL) [7], [8] and one/few shot learning techniques [9], [10], [10], [11], [12] are thus proposed to overcome such limitations. In contrast to train the supervised DNNs, ZSL is to learn the capability of transferring the relevant knowledge from known objects to knowledge-less or unknown ones.

ZSL has recently received wide attention in recent various studies [8], [13], [14], [15], [16], [17], [18], [19], [20]. It aims to recognize the objects with no corresponding labeled sample (unseen objects) from the knowledge obtained from the objects with considerable number of training samples (seen objects). In order to transfer the knowledge from seen classes to unseen ones, there is a common assumption that the side information about each class is available, such as class attributes [8], [21], [22] or word vectors [7], [22].

When both seen and unseen class names are embedded in the semantic word vectors space, it is then called class prototypes [23]. Since the distance between word vector or class attributes are measurable, and the visual features could also be projected onto semantic space, the idea of ZSL is to learn a general mapping or relationships between the visual features and side information from labelled seen classes and then apply it to the unseen classes. Recognizing unseen object is performed by projecting the visual features of unseen classes into the semantic spaces by learnt mapping and assign the label by a simple nearest neighbour (NN) search, which becomes a classical classification problem.

Most existing ZSL models [7], [8], [15], [22], [24], [25], [26], [27], [28], [29] mainly focus on the projection between visual and semantic features, when the reconstruction of the original feature is not taken into account. Although seen and unseen classes share some overlapping domain, this may lead to the problem of projection domain shift. Kodirov et. al [30] recently proposed a novel method, called Semantic AutoEncoder (SAE), which includes a reconstruction constraint for the original visual features. Such a projection not only includes the mapping from the visual to semantic spaces, but also preserves the information for recovering the original visual features, mitigating the domain shift problem. After that, Liu et. al [31] restricted the projection function in SAE to be low-rank to enhance the robustness. Even though the reconstruction of visual features demonstrates its capability of alleviating the domain shift problem, [30] and [31] are still indeed the way to directly project features between visual and semantic space. All above methods do not exploit the instinct mapping structure between the visual and semantic space. In general, when people observe an unknown object, they usually first search the similar concepts in mind, and then match it with the same concept, vice versa. These

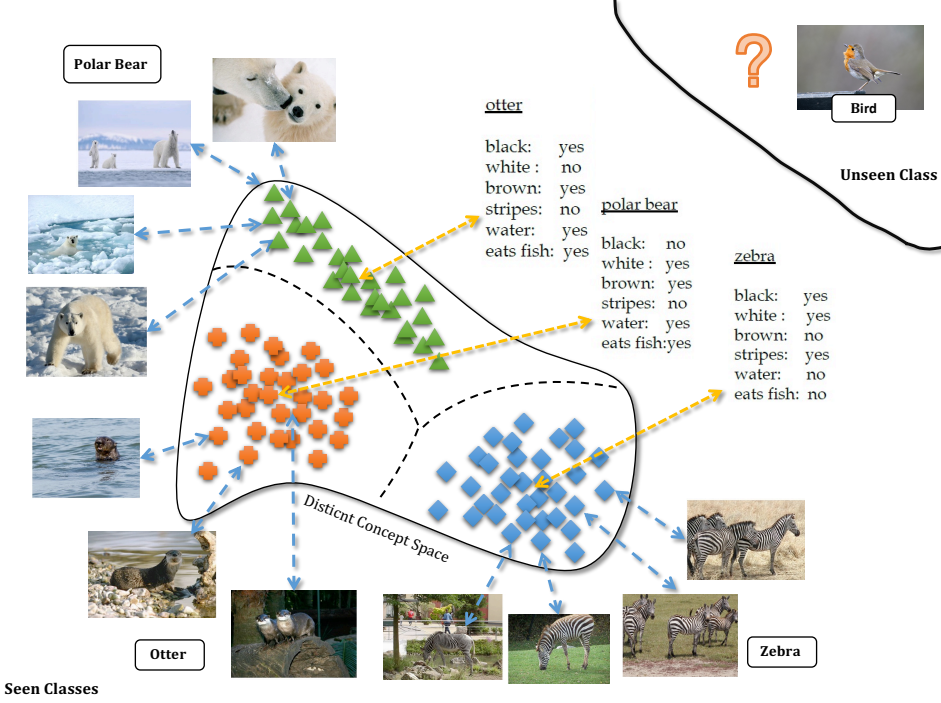


Fig. 1: The Illustration of JCMSPL.

concepts have a class-to-class map on both of the visual and semantic features. Therefore, in this paper, we purpose a novel method named Joint Concept Matching-Space Projection Learning (JCMSPL) to mimic such human thinking behavior and take the advantage of the self-reconstruction to confront with the domain shift issue. We assume there is a common concept space incorporating distinct class concepts by introducing the class-specific information, and both visual and semantic features could be precisely projected and reconstructed by such common and distinct concepts. Hence, in such a way, the domain-invariant is introduced by the distinct concept mapping and the self-reconstruction of both visual and semantic features. In addition, such distinct common concept space can precisely match visual and semantic features of each class one to one.

To have a more clear intuition, our purposed method is illustrated in Figure 1. As shown in Figure 1, different categories in the visual space have many overlaps of colors and backgrounds, such as the similar color of the otter and the zebra, the same sea background of the polar bear and the otter, which results in an indivisible issue among different classes. Similarly, in the semantic space, many objects also share common attributes. For examples, both the otter and the polar bear have brown, water and eats fish tags. Thus, a distinct concept space is adopted, where both visual and semantic features of these seen classes are projected as separable concepts. Meanwhile, the visual and semantic features of each class are one-to-one matched them, which is also how human to associate the visual with words. Additionally, when looking at the unseen classes (such as, birds), it has much different features in both visual and semantic space comparing to the seen classes (such as, otter, polar bear and zebra), and also causes domain gap between

seen and unseen classes. In order to mitigate such effects, the reconstructions of both visual and semantic features are also included, which are illustrated by the dash-line two-way arrows in Figure 1.

Our main contributions are summarized as follows:

- A novel ZSL is proposed based on the intermediate common concept space with class-specific information to well match visual and semantic features.
- Both visual and semantic feature can be reconstructed by the common concept space to mitigate the domain-shift problem.
- An efficient algorithm based on Sylvester equation is developed, which achieves state-of-arts performances on four benchmark datasets for ZSL and generalized ZSL.

The balance of the paper is organized as follows: In Section 2, we review the literature and background of relevance to this paper. We define the problem, formulate our novel approach and propose its algorithmic solution and recognition scheme in Section 3. Substantiating experimental results and evaluations as well as the convergence and complexity analysis are presented in Section 4. Finally, we provide some concluding remarks in Section 5.

2 RELATED WORK

2.1 Class-specific Information

In order to improve classification accuracy, the supervised learning methods [32], [33] incorporate class-specific information to make the classifier more discriminative, which looks like a diagonal-block matrix or a simple binary label matrix. In both [32], [33], the class-specific information makes the labels more consistent and distinct to each other.

In this paper, we also introduce a similar class-specific information matrix (a diagonal-block matrix) as a support to make the common space more distinct for different classes. That is to force the projected visual and semantic features of different classes to be discriminative enough.

2.2 Projection Learning

Various ZSL methods have been recently proposed, which are mainly divided into three groups based on different projection methods. (1) The first group employ a projection function from a visual space to a semantic space, and subsequently determine the class labels in the semantic space. The projection function can be conventional regression models [8], [24] or a deep neural network [7], [22], [25], [26]. This kind of projection methods is regarded as a forward projection Learning. (2) As opposed to the first group, the second one is to learn the reverse projection function from the semantic space to the feature space [15], [27], [28], [29] to alleviate the well-known hubness problem in the nearest neighbor search in high-dimensional spaces [34]. (3) The third group projects both the visual and semantic features to a intermediate space [16], [35], [36]. Our proposed JCMSPL model adopts a similar intermediate space where both visual and semantic features are projected. JCMSPL further employs two reconstruction constraints based on it. By using the intermediate space, the visual features can be projected into the semantic space, and vice versa. Therefore, JCMSPL can be treated as a combination of all these three groups, which indirectly integrates both forward and reverse projections with an intermediate space for ZSL with additional class-specific knowledge.

2.3 Projection Domain Shift

According to the aforementioned domain shift problem that first mentioned in [23], there are two versions of the ZSL problems has been discussed in the literature. One is inductive ZSL [30], [31], where the projection function only relies on the seen classes, when all the unseen data is only used for testing. Another is transductive ZSL [27], [37], [38], which incorporates the unlabelled unseen classes into projection function learning to alleviate the domain shift problem. Our JCMSPL is based on the inductive ZSL and only uses the reconstruction constraints of both visual and semantic feasters and class-specific information to deal with domain shift problem.

3 METHODOLOGY

3.1 Notation

Uppercase and lowercase bold letters respectively denote matrices and vectors throughout the paper. The transpose and inverse of matrices are respectively represented by the superscripts T and -1 , such by \mathbf{A}^T and \mathbf{A}^{-1} . The identity matrix and all-zero matrix respectively denoted as \mathbf{I} and $\mathbf{0}$.

3.2 Problem Definition

The goal of ZSL is to assign the unseen class label to the unseen samples, and both unseen labels and samples are independent from the training phase.

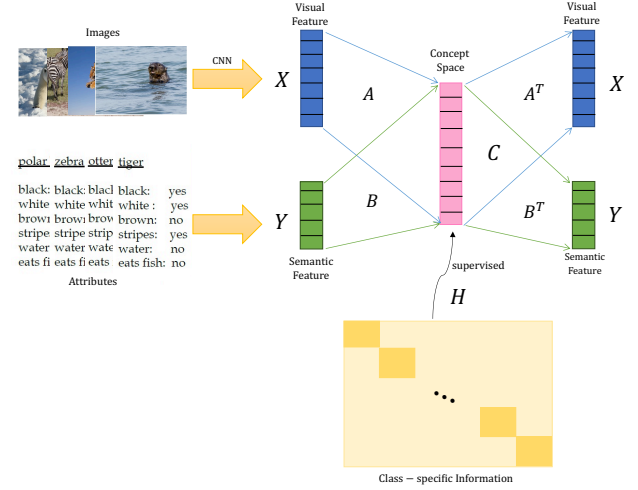


Fig. 2: The framework of our purposed JCMSPL is comprised of 3 procedures. (I) A CNN is first used to extract the visual features \mathbf{X} , such as GoogleNet [39], VGG-19 [3] and ResNet101 [5], and then project them by the function \mathbf{A} into the common concept space \mathbf{C} . Finally, \mathbf{A}^T is employed to reconstruct the \mathbf{X} from concept space \mathbf{C} . (II) The attributes/word vector \mathbf{Y} is used to embed the different classes into the semantic space. The project function \mathbf{B} maps the semantic feature \mathbf{Y} into the common concept space \mathbf{C} as well, and \mathbf{B}^T reconstruct \mathbf{Y} from \mathbf{C} . (III) A block-diagonal matrix \mathbf{H} supervise and support the common concept space \mathbf{C} to be distinct and separable, where the light-yellow part shown in the class-specific information is with all entrances of 0 and the dark-yellow part is occupied by the elements of 1.

Let $S = \{\mathbf{X}_s, \mathbf{Y}_s, L_s\}$ denote the set of seen classes with c_s seen classes and n_s labeled samples. And let $U = \{\mathbf{X}_u, \mathbf{Y}_u, L_u\}$ denote the set of unseen classes with c_u seen classes and n_u labeled samples. $\mathbf{X}_s \in \mathbf{R}^{m \times n_s}$ and $\mathbf{X}_u \in \mathbf{R}^{m \times n_u}$ are m -dimensional visual features samples in the seen and unseen sets, $\mathbf{Y}_s \in \mathbf{R}^{d \times n_s}$ and $\mathbf{Y}_u \in \mathbf{R}^{d \times n_u}$ are associated class-level attributes, namely semantic features. L_s, L_u are respectively the corresponding label sets of seen and unseen classes. Based on the definition of ZSL, the labels of seen and unseen sets have no overlap, i.e., $L_s \cap L_u = \emptyset$, and ZSL aims to learn a classifier $f : \mathbf{X}_u \rightarrow L_u$, so as to predict the label for unseen classes, where f is learnt only based on the seen class sets $S = \{\mathbf{X}_s, \mathbf{Y}_s, L_s\}$.

3.3 Model Formulation

As mentioned in Section 1, JCMSPL incorporates a distinct common concept space with class-specific information, and both visual and semantic features self-reconstructions. Therefore, JCMSPL consists of 3 procedures as illustrated in Figure 2, and formulated as follows:

$$\begin{aligned} \min_{\mathbf{A}, \mathbf{B}, \mathbf{C}} \frac{1}{2} \|\mathbf{A}\mathbf{X}_s - \mathbf{C}\|_F^2 + \frac{\lambda_1}{2} \|\mathbf{B}\mathbf{Y}_s - \mathbf{C}\|_F^2 + \frac{\lambda_2}{2} \|\mathbf{C} - \mathbf{H}\|_F^2 \\ + \frac{\lambda_3}{2} \|\mathbf{X}_s - \mathbf{A}^T \mathbf{C}\|_F^2 + \frac{\lambda_4}{2} \|\mathbf{Y}_s - \mathbf{B}^T \mathbf{C}\|_F^2, \end{aligned} \quad (1)$$

where $\mathbf{A} \in \mathbf{R}^{k \times m}$ is the projection matrix from the visual space to the common space $\mathbf{C} \in \mathbf{R}^{k \times n_s}$, while $\mathbf{B} \in \mathbf{R}^{k \times d}$ is the projection matrix from semantic space to the common space. We further require the transpose matrices \mathbf{A}^T and \mathbf{B}^T to be respectively the reverse projection matrix from the common space \mathbf{C} to the visual and semantic spaces, so that visual and semantic features can also be reconstructed by the common space. $\mathbf{H} \in \mathbf{R}^{k \times n_s}$ is a diagonal-block matrix, predefined by the class-specific information to make the common concept space distinct and enhance the matching of each class more accuracy. $\lambda_1 - \lambda_4$ are the turning parameters.

3.4 Algorithmic Solution

Since the objective function in Eq. (1) is a multi-convex problem, we may reliably update the variables by a block-coordinate descent method.

Update A: When \mathbf{B} and \mathbf{C} are fixed, \mathbf{A} is updated by

$$\mathbf{A}^*_{t+1} = \arg \min_{\mathbf{A}} \frac{1}{2} \|\mathbf{A} \mathbf{X}_s - \mathbf{C}_t\|_F^2 + \frac{\lambda_3}{2} \|\mathbf{X}_s - \mathbf{A}^T \mathbf{C}_t\|_F^2. \quad (2)$$

As $\|\mathbf{Z}\|_F = \|\mathbf{Z}^T\|_F$, the Eq.(2) is re-organized as

$$\mathbf{A}^*_{t+1} = \min_{\mathbf{A}} \frac{1}{2} \|\mathbf{A} \mathbf{X}_s - \mathbf{C}_t\|_F^2 + \frac{\lambda_3}{2} \|\mathbf{X}_s^T - \mathbf{C}_t^T \mathbf{A}\|_F^2. \quad (3)$$

Then, taking the derivative of Eq. (3) and setting it to zero, we obtain:

$$\lambda_3 \mathbf{C}_t \mathbf{C}_t^T \mathbf{A}^*_{t+1} + \mathbf{A}^*_{t+1} \mathbf{X}_s \mathbf{X}_s^T = (1 + \lambda_3) \mathbf{C}_t \mathbf{X}_s^T. \quad (4)$$

Denote,

$$\mathbf{M}_A = \lambda_3 \mathbf{C}_t \mathbf{C}_t^T,$$

$$\mathbf{N}_A = \mathbf{X}_s \mathbf{X}_s^T,$$

$$\mathbf{T}_A = (1 + \lambda_3) \mathbf{C}_t \mathbf{X}_s^T,$$

we have:

$$\mathbf{M}_A \mathbf{A}^*_{t+1} + \mathbf{A}^*_{t+1} \mathbf{N}_A = \mathbf{T}_A, \quad (5)$$

To solve Eq. (5), we use the following definition and theorems:

Definition 1. A Sylvester equation [40] is a matrix equation of the following form:

$$\mathbf{RZ} + \mathbf{ZS} = \mathbf{T}. \quad (6)$$

When \mathbf{R} , \mathbf{S} and \mathbf{T} are given, the problem is to find the possible matrices \mathbf{Z} that obey this equation.

Theorem 2. The sufficient condition of Eq. (6) to have a solution \mathbf{Z} is that:

The matrix $\begin{bmatrix} \mathbf{R} & \mathbf{0} \\ \mathbf{0} & \mathbf{S} \end{bmatrix}$ is similar to the matrix $\begin{bmatrix} \mathbf{R} & \mathbf{T} \\ \mathbf{0} & -\mathbf{S} \end{bmatrix}$.

Theorem 3. The sufficient condition for Eq. (6) to have a unique solution \mathbf{Z} is that:

The eigenvalues $(\sigma_1^R, \sigma_2^R, \dots, \sigma_r^R)$ of \mathbf{R} and the eigenvalues $(\sigma_1^S, \sigma_2^S, \dots, \sigma_s^S)$ of \mathbf{S} satisfy that $\sigma_i^R \neq -\sigma_j^S, \forall i = 1, \dots, r, \forall j = 1, \dots, s$.

More details and proofs of Definition 1, Theorem 1 and 2 can be found in [41].

By Definition 1, Eq. (5) is a Sylvester equation and easy to meet the sufficient and unnecessary condition in Theroem 3, as ZSL is based on real image data. Eq. (5) is

thus solved efficiently by the Bartels-Stewart algorithm [42], which can be implemented by a single line code: Sylvester in MATLAB¹.

Update B: When \mathbf{A} and \mathbf{C} are fixed, \mathbf{B} is updated by

$$\mathbf{B}^*_{t+1} = \arg \min_{\mathbf{B}} \frac{\lambda_1}{2} \|\mathbf{B} \mathbf{Y}_s - \mathbf{C}_t\|_F^2 + \frac{\lambda_4}{2} \|\mathbf{Y}_s - \mathbf{B}^T \mathbf{C}_t\|_F^2. \quad (7)$$

Similar to update \mathbf{A} , we have the Sylvester equation related to \mathbf{B} :

$$\mathbf{M}_B \mathbf{B}^*_{t+1} + \mathbf{B}^*_{t+1} \mathbf{N}_B = \mathbf{T}_B, \quad (8)$$

where

$$\mathbf{M}_B = \lambda_4 \mathbf{C}_t \mathbf{C}_t^T,$$

$$\mathbf{N}_B = \lambda_1 \mathbf{Y}_s \mathbf{Y}_s^T,$$

$$\mathbf{T}_B = (\lambda_1 + \lambda_4) \mathbf{C}_t \mathbf{Y}_s^T.$$

Update C: When \mathbf{A} and \mathbf{B} are fixed, \mathbf{C} is updated by

$$\begin{aligned} \mathbf{C}^*_{t+1} = & \arg \min_{\mathbf{C}} \frac{1}{2} \|\mathbf{A}_{t+1} \mathbf{X}_s - \mathbf{C}\|_F^2 + \frac{\lambda_1}{2} \|\mathbf{B}_{t+1} \mathbf{Y}_s - \mathbf{C}\|_F^2 \\ & + \frac{\lambda_2}{2} \|\mathbf{C} - \mathbf{H}\|_F^2 + \frac{\lambda_3}{2} \|\mathbf{X}_s - \mathbf{A}^T \mathbf{C}\|_F^2 \\ & + \frac{\lambda_4}{2} \|\mathbf{Y}_s - \mathbf{B}^T \mathbf{C}\|_F^2, \end{aligned} \quad (9)$$

Derivative Eq. (9) and setting it to zero, and its analytical solution is as following:

$$\begin{aligned} \mathbf{C}^*_{t+1} = & ((1 + \lambda_1 + \lambda_2) \mathbf{I} + \lambda_3 \mathbf{A}_{t+1} \mathbf{A}^T_{t+1} + \lambda_4 \mathbf{B}_{t+1} \mathbf{B}^T_{t+1})^{-1} \\ & (\lambda_2 \mathbf{H} + (1 + \lambda_3) \mathbf{A}_{t+1} \mathbf{X}_s + (\lambda_1 + \lambda_4) \mathbf{B}_{t+1} \mathbf{Y}_s). \end{aligned} \quad (10)$$

We follow the updating steps in each iteration of our algorithm, which are summarized in Algorithm 1.

Algorithm 1 Joint Concept Matching-Space Projection Learning

Input: Visual features training set \mathbf{X}_s , semantic features training set \mathbf{Y}_s , tuning parameters $\lambda_1 - \lambda_4$, and maximum iteration t_{MAX} .

Output: The visual projection function \mathbf{A} , the semantic projection function \mathbf{B} and the distinct common space \mathbf{C} .

- 1: Initialize \mathbf{A} , \mathbf{B} and \mathbf{C} as random matrices;
- 2: **while** not converged **and** $t < t_{MAX}$ **do**
- 3: $t = t + 1$;
- 4: Update \mathbf{A}_t by solving Eq. (5);
- 5: Update \mathbf{B}_t by solving Eq. (8);
- 6: Update \mathbf{C}_t by Eq. (10);
- 7: **end while**

1. <https://www.mathworks.com/help/matlab/ref/sylvester.html>

3.5 Zero-shot Recognition

After we obtain the projection matrices \mathbf{A} and \mathbf{B} , zero-shot recognition can be subsequently performed in two ways:

- (1) With projection matrices \mathbf{A}^T and \mathbf{B} , when a new test sample $\mathbf{y}_{u_i} \in \mathbf{Y}_u$ is given, the associated visual feature $\hat{\mathbf{x}}_{u_i}$ of unseen class are easily reconstructed by the semantic features thorough following method:

$$\hat{\mathbf{x}}_{u_i} = \mathbf{A}^T \mathbf{B} \mathbf{y}_{u_i}. \quad (11)$$

The test data in the visual space can be classified by a simple Nearest Neighbour (NN) classifier based on the distance between the estimated visual representation $\hat{\mathbf{x}}_{u_i}$ and the prototype projections in the visual space \mathbf{X}_u . The label l_{u_i} for the unseen sample is assigned by:

$$l_{u_i} = \min_{c_j} D(\hat{\mathbf{x}}_{u_i}, \mathbf{X}_{u_{c_j}}); \quad (12)$$

where $\mathbf{X}_{u_{c_j}}$ is the c_j -th unseen class prototype projected in the feature space, D is an arbitrary distance function.

- (2) With projection matrices \mathbf{A} and \mathbf{B}^T , when a new test sample $\mathbf{x}_{u_i} \in \mathbf{X}_u$ is given, the associated semantic feature $\hat{\mathbf{y}}_{u_i}$ of unseen class are easily reconstructed by the visual features thorough following method:

$$\hat{\mathbf{y}}_{u_i} = \mathbf{B}^T \mathbf{A} \mathbf{x}_{u_i}. \quad (13)$$

The test data in the semantic space can be classified by a simple Nearest Neighbour (NN) classifier based on the distance between the estimated semantic representation $\hat{\mathbf{y}}_{u_i}$ and the prototype projections in the semantic space \mathbf{Y}_u . The label l_{u_i} for the unseen sample is assigned by:

$$l_{u_i} = \min_{c_j} D(\hat{\mathbf{y}}_{u_i}, \mathbf{Y}_{u_{c_j}}), \quad (14)$$

where $\mathbf{Y}_{u_{c_j}}$ is the prototype attribute vector of the c_j -th unseen class, D is an arbitrary distance function.

In our experiments, the results of both strategies are reported.

4 EXPERIMENTS

4.1 Datasets and Settings

4.1.1 Datasets

Four benchmark datasets are used to evaluate the state-of-arts and our method. Animals with Attributes (AwA) [8], CUB-200-2011 Birds (CUB) [43], and SUN Attribute (SUN) [44] are three widely used medium-scale datasets in existing ZSL works. But they are not large enough to show the capability of the original motivation of ZSL for scaling up visual recognition. Thus, the ILSVRC2012/ILSCRC2012 (ImNet) [1] is then selected as a large-scale dataset in [45].

AwA [8] consists of 30475 images of 50 animals classes with 85 associated class-level attributes, which is a coarse-grained dataset. 40 classes are used for training, while the rest 10 classes with 6180 images are used for testing.

CUB [43] is fine-grained dataset with 11788 images for 200 different type of bird species that annotated by 312

attributes. The first standard zero-shot split was introduced in [19], where 150 classes are for training and 50 classes are for testing.

SUN [44] is also a fine-grained datasets, which includes 14340 images for 717 types of different scenes categories that annotated by 120 attributes. Following the split in [8] 645 out of 71 classes are used as training set and the rest 72 classes are for testing.

ImNet [1] contains 218000 images and 1000-dimensional class-level attributes. Following the split in [45], the 1000 classes of ILSVRC2012 are used as seen classes, when the 360 classes of ILSVRC2010 are used as unseen classes, which are not included in ILSVRC2012.

For fair comparisons against published results, we use the same above training (seen) and testing (unseen) splits for our ZSL evaluation. The summary of all those datasets are listed in the Table 1.

TABLE 1: The details of four evaluated datasets. Notation: 'SS'- the semantic space; 'A'- the attribute, 'W'- the word vector; 'SS-D'- the dimension of the semantic space.

Datasets	#Images	SS	SS-D	# Seen/#Unseen Classes
AwA [8]	30475	A	85	40/10
CUB [43]	11788	A	312	150/50
SUN [44]	14340	A	64	645/72
ImNet [1]	218000	W	1000	1000/360

4.1.2 Semantic Spaces

Generally, there are two different types of attributes. One is the attribute annotations, which is for the medium datasets, and another one is the word vector representation, which is used for large-scale datasets. The word vector, word2vec [46], representation is obtained by training a skip-gram text model on a corpus of 4.6M Wikipedia documents.

4.1.3 Visual Spaces

In recent ZSL modes, all the visual features are extracted from Convolutional Neural Networks (CNNs) [3], [5], [39] that are pre-trained by the 1K classes in ILSVRC 2012 [1]. In our experiments, the visual features are extracted from pre-trained GoogleNet [39]. It is worthy noting that the visual features used in most compared methods are GoogleNet features, except the Table 2, where a number of most ZSL models used VGG19 [3] and ResNet101 [5] features. Since the source codes of such models are not released, we can not report the results based on GoogleNet, instead the results reported in the original paper are listed in the Table 2. But note that, as demonstration in [47], the VGG19 and ResNet101 features usually obtain better performances than the GoogLeNet features in the ZSL task. Since we use GoogleNet features which are not stronger features, it is fair for such comparisons in the Table 2.

4.1.4 Parameter Settings

In JCMSPL, there are four tuning parameters $\lambda_1 - \lambda_4$ in Eq . (1). Following [15], [30], the parameters are tuned by class-wise cross-validation of the training set. As SUN dataset has multiple splits, in our experiments, we report the average performance of the same splits that used in [16].

TABLE 2: The standard ZSL classification accuracy (%). For ImNet, hit @5 is reported. For visual Features: G - GoogleNet [39]; V - VGG19 [3]; R - ResNet101 [5].

Medium Datasets					Large Dataset		
Method	V-Features	AwA	CUB	SUN	Method	V-Features	ImNet
RPL [15]	G	80.4	52.4	-	DeViSE [22]	G	12.8
SSE [50]	V	76.3	30.4	-	ConSE [51]	G	15.5
SJE [24]	G	73.9	51.7	56.1	AMP [52]	G	13.1
JLSE [36]	V	80.5	42.1	-	SS-Voc [45]	G	16.8
SynC [16]	G	72.9	54.7	62.7	SAE [30]	G	27.2
SAE [30]	G	84.7	61.4	65.2	CVA [53]	V/R	24.7
LAD [54]	V	82.5	56.6	-	VSZL [55]	V	23.1
SCoRe [56]	V	73.9	51.7	-	LESAE [31]	G	27.6
LESD [57]	V/G	82.8	56.2	-			
CVA [53]	V/R	71.4	52.1	61.7			
f-CLSWGAN [58]	R	69.9	61.5	64.5			
VSZL [55]	V	85.3	57.4	-			
LESAE [31]	R	66.1	53.9	60.0			
AAW [59]	V	83.3	38.4	-			
LSD [60]	V	82.7	58.5	-			
BZSL [61]	V/G	80.5	56.3	-			
JCMSP (V → S)	G	77.5	60.0	66.3	JCMSP (V → S)	G	26.0
JCMSP (S → V)	G	86.2	62.6	54.1	JCMSP (S → V)	G	27.5

4.1.5 ZSL Settings

Standard ZSL: The standard ZSL setting is widely used in recent ZSL works [24], [25]. The seen and unseen classes are split following the Table 1.

Generalized ZSL: The generalized ZSL setting emerges recently [48], [49], whose testing set includes both seen and unseen samples. Such setting is more clear to reflect the real-world scenarios.

4.1.6 Evaluation Metrics

Standard ZSL: The multi-way classification accuracy as previous works is used for three medium-scale datasets, when the flat hit @K classification accuracy as in [45] is used for the large-scale dataset. Hit @K means that for a testing sample, the top K assigned labels should include the correct label. In the experiment, hit @5 accuracy is reported for over all test samples.

Generalized ZSL: Three metrics are used in the generalized ZSL. The first one is acc_s , the accuracy of classifying the seen samples to the all classes, which includes both seen and unseen samples. The second one is, acc_u the accuracy of classifying the unseen samples to the all classes. The third one is HM , which is the harmonic mean of acc_s and acc_u , i.e.,

$$HM = \frac{2 \times acc_s \times acc_u}{acc_s + acc_u}.$$

4.1.7 Competitive Methods

16 existing ZSL methods are used for performance comparison for three medium-scale datasets and 8 state-of-arts are used for the large-scale ones, where RPL [15], SSE [50], SJE [24], JLSE [36], SynC [16], SAE [30], LAD [54], SCoRe [56], LESD [57], CVA [53], f-CLSWGAN [58], VSZL [55], LESAE [31], AAW [59], LSD [60] and BZSL [61] are used

for medium-scale ones, and DeViSE [22], ConSE [51], AMP [52], SS-Voc [45], SAE [30], CVA [53], VSZL [55], and LESAE [31] are used for the large one. These ZSL methods cover a wide range of recent and representative ZSL models and achieve the state-of-the-art results.

4.2 Experiment Results

4.2.1 Standard ZSL

The comparative result of various datasets under standard ZSL settings are listed in Table 2. All these results of comparison methods are based on inductive ZSL. That is, no unlabeled unseen samples are incorporated in the training phase. Based on Table 2, our method achieve the best results on all three medium-scale datasets and a comparable result on the large dataset, which demonstrates that the reconstructions of both visual and semantic mitigate the domain shift problem and the class-specific distinct common space make the visual and semantic features match more precisely. For all three medium datasets, our method improves about 1% performance over the strongest competitors. For the large dataset, although our method is only slightly lower than the LESAE, it is still much better than other competitive methods.

4.2.2 Generalized ZSL

Following the same setting of [18], we extract out 20% seen classes data samples and mix them with the unseen classes samples. The generalized ZSL of AwA and CUB are listed in Table 3, which includes 6 competitive methods. Although the HM score of AwA is slightly lower than SAE, it is still comparable and its acc_u , the unseen to all class classification accuracy, is still higher than SAE, which demonstrate a better generalization capability. For CUB dataset, our method achieves the highest HM and acc_u , which again shows that our method is benefit for the generalized ZSL setting. The

TABLE 3: The comparative results(%) of generalized ZSL as setting in [18]. All the results are tests on GoogleNet visual features.

Method	AwA			CUB		
	acc_s	acc_u	HM	acc_s	acc_u	HM
DAP [8]	77.9	2.4	4.7	55.1	4.0	7.5
IAP [8]	76.8	1.7	3.3	69.4	1.0	2.0
ConSE [51]	75.9	9.5	16.9	69.9	1.8	2.5
APD [48]	43.2	61.7	50.8	23.4	39.9	29.5
GAN [49]	81.3	32.3	46.2	72.0	26.9	39.2
SAE [30]	67.6	43.3	52.8	36.1	28.0	31.5
JCMSPL (ours)	48.3	56.4	52.1	54.2	50.7	52.4

high accuracy for acc_s reflects that the method is overfitting when training for seen classes and is difficult to generalize to unseen ones.

4.3 Further Evaluations

4.3.1 Ablation Study

Our JCMSPL model can also be simplified as follows:

(1) When $\lambda_2 = 0$, then the class-specific information is not used, our JCMSPL degrades to the joint space projection with reconstruction, and denoted as JCM-SPL1, *i.e.*,

$$\min_{\mathbf{A}, \mathbf{B}, \mathbf{C}} \frac{1}{2} \|\mathbf{AX}_s - \mathbf{C}\|_F^2 + \frac{\lambda_1}{2} \|\mathbf{BY}_s - \mathbf{C}\|_F^2 + \frac{\lambda_3}{2} \|\mathbf{X}_s - \mathbf{A}^T \mathbf{C}\|_F^2 + \frac{\lambda_4}{2} \|\mathbf{Y}_s - \mathbf{B}^T \mathbf{C}\|_F^2.$$

(2) When $\lambda_3 = 0$ and $\lambda_4 = 0$, the class-specific information is used, but the reconstructions of both visual and semantic space are not taken in account. Our JCMSPL degrades to the joint concept matching space projection without reconstruction, which denoted as JCM-SPL0, *i.e.*,

$$\min_{\mathbf{A}, \mathbf{B}, \mathbf{C}} \frac{1}{2} \|\mathbf{AX}_s - \mathbf{C}\|_F^2 + \frac{\lambda_1}{2} \|\mathbf{BY}_s - \mathbf{C}\|_F^2 + \frac{\lambda_2}{2} \|\mathbf{C} - \mathbf{H}\|_F^2.$$

This is similar to the third group of projection learning in the literature but with the classes information.

(3) When $\lambda_2 = 0$, $\lambda_3 = 0$ and $\lambda_4 = 0$, both the class-specific information and the reconstructions of both visual and semantic space are not used. Our JCM-SPL then degrades to the joint concept matching space projection without reconstruction and any class-specific information, which is similar to the third group of projection learning in the literature [16], [36]. This is denoted as intermediate space projection learning (IPL), *i.e.*,

$$\min_{\mathbf{A}, \mathbf{B}, \mathbf{C}} \frac{1}{2} \|\mathbf{AX}_s - \mathbf{C}\|_F^2 + \frac{\lambda_1}{2} \|\mathbf{BY}_s - \mathbf{C}\|_F^2.$$

(4) When $\lambda_1, \lambda_2, \lambda_3$ and $\lambda_4 = 0$ and using the semantic space instead of the intermediate/common space,

JCM-SPL is finally degrades to the original forward projection learning method [24], denoted as FPL, *i.e.*,

$$\min_{\mathbf{A}} \frac{1}{2} \|\mathbf{AX}_s - \mathbf{Y}_s\|_F^2.$$

To evaluate the contribution of purposed Full JCM-SPL method, its simple degraded FPL, IPL, JCM-SPL0, JCM-SPL1 are compared with same standard splits of AwA and CUB datasets. The standard ZSL accuracy of hereabove simple JCM-SPL methods are listed and shown in Table 4 and Fig. 3.

TABLE 4: The evaluation of the contributions of JCM-SPL and the importance of both reconstruction constraint and class-specific information.

Projection Method	AwA	CUB
FPL	72.7%	40.2%
IPL	77.1%	46.5%
JCM-SPL0	82.4%	60.3%
JCM-SPL1	84.7%	61.6%
Full JCM-SPL	86.2%	62.6%

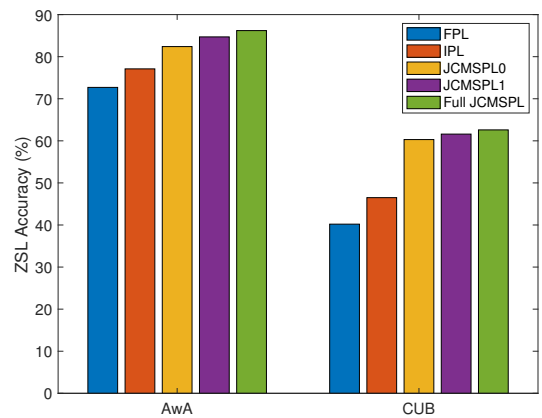


Fig. 3: Ablation study results of standard ZSL on two medium-scale datasets.

The ablation study results shows that: (1) When comparing the IPL and FPL, it shows that the intermediate space respectively brings 4.4% and 6.3% improvements for AwA and CUB datasets. The commons space introduces the latent representations of both visual and semantic features that enhance their similarities. (2) The result of JCM-SPL0 = IPL + class-specific information also has 5% – 13% gains comparing to IPL, which validate the effectiveness of class-specific information. Even when the results are already high enough, the class-specific information also introduce a exceeding 1% gains, as comparing JCM-SPL1 with Full JCM-SPL. Class-specific latent space well matches the visual and semantic features class-to-class. (3) As the shown result of JCM-SPL1 = IPL + reconstructions vs. IPL, both reconstructions of visual and semantic features are important for ZSL, which results 7% – 14% improvements. (4) To combine with all these class-specific information and feature reconstructions, our Full JCM-SPL has significant improvements ranging from

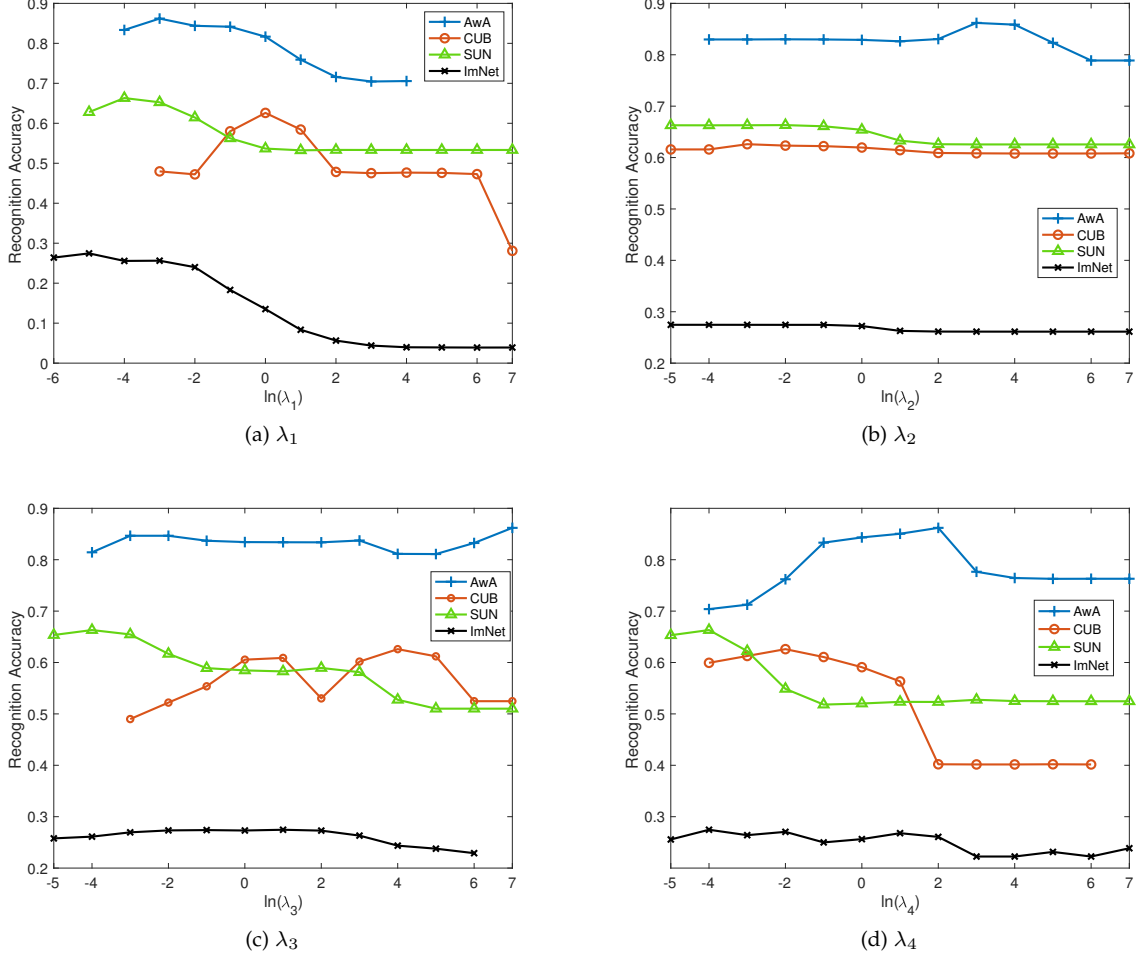


Fig. 4: Parameters analysis for $\lambda_1 - \lambda_4$.

9% – 16% when comparing to IPL and achieves 1% – 2% improvements when comparing to JCMSPL1, the one only with such reconstruction constraints.

4.3.2 Parameters Analysis

Figure 4 shows that the value of $\lambda_1 - \lambda_4$ that achieves the best performance in different datasets. The detailed settings of four benchmark datasets are listed in Table 5.

TABLE 5: The parameters $\lambda_1 - \lambda_4$ settings are used for four different datasets.

Parameter	AwA	CUB	SUN	ImNet
λ_1	$1e - 3$	1	$1e - 4$	$1e - 5$
λ_2	$1e3$	$1e - 3$	$1e - 2$	$1e - 5$
λ_3	$1e7$	$1e4$	$1e - 4$	$1e1$
λ_4	$1e2$	$1e - 1$	$1e - 4$	$1e - 4$

First we evaluate the weight of mapping the semantic features to common distinct space by tuning the λ_1 during our algorithm training phase. Since visual features have different structures from semantic features, the weights of both visual feature mapping and semantic features mapping should be different, too. In Figure 4a, it shown that our

algorithm achieves better performance, when the weights of semantic feature mapping is in the range of $[10^{-5}, 10]$ for all four datasets.

We then evaluate λ_2 , the influence of class-specific information term during training. From the evaluation in Figure 4b, it is witnessed that the classification accuracy tends to be better during the range of $[10^2, 10^6]$ for AwA, the range of $[10^{-3}, 10^{-2}]$ for CUB, the range of $[10^{-5}, 10^{-2}]$ for SUN and the range of $[10^{-5}, 1]$ for ImNet. Comparing with the magnitude of other parameters in each dataset, the class-specific information term has large weights for AwA and SUN datasets, which brings the distinct knowledge of different class for a better matching between visual and semantic features. Although its weight is small for CUB dataset, the accuracy drops when its weight λ_2 decreases. This validates that the class-specific information term is also helpful for zero-shot recognition to be robust against the domain shift issue and match the same class visual and semantic features.

In addition, through the analysis on parameter λ_3 and λ_4 (Figure 4c and 4c), they show that the ranges of both λ_3 and λ_4 that obtain promising performances are respectively less than 10^8 and 10^3 on four datasets. Although four different datasets have different magnitudes, the λ_3 and

λ_4 are relatively larger than λ_1 and λ_2 (the detailed values is listed in Table 5). This shows that the reconstructions of both visual and semantic features can improve the zero-shot learning ability, narrow the domain shift gap and explore more intrinsic structure within seen data.

4.3.3 Convergence and Complexity Analysis

Convergence Analysis: In light of the non-convexity of Eq. (1), the convergence of our algorithm is not guaranteed by standard results. We hence separately prove the convergence of our algorithm: let $f(\mathbf{A}, \mathbf{B}, \mathbf{C})$ be the loss function of Eq. (1), then the following result follows.

Theorem 4. *The sequence $\{\Theta_t = (\mathbf{A}_t, \mathbf{B}_t, \mathbf{C}_t)\}_{t=1}^{\infty}$ converges to the following set of bounded feasible stationary points of the loss function f* ²

$$S = \{\Theta = (\mathbf{A}_t, \mathbf{B}_t, \mathbf{C}_t) \mid \|\Theta\| < R\}.$$

The Theorem 4 shows that our Algorithm 1 not only converges, but also generates a solution sequence and eventually converges to the stationary points of the underlying optimization. Theorem 4 has been proved in the Appendix A.

Complexity Analysis: Since the solution complexity of sylvester equation only depends on the dimension of rows, the complexities of updating \mathbf{A} and \mathbf{B} only related with the dimension of features, but instead of the sample size n . That is, the complexities of updating \mathbf{A} and \mathbf{B} are respectively $O(m^3)$ and $O(d^3)$, while the complexity of updating \mathbf{C} is $O(k^3 + k^2m + k^2d + kmn_s + kdn_s)$.

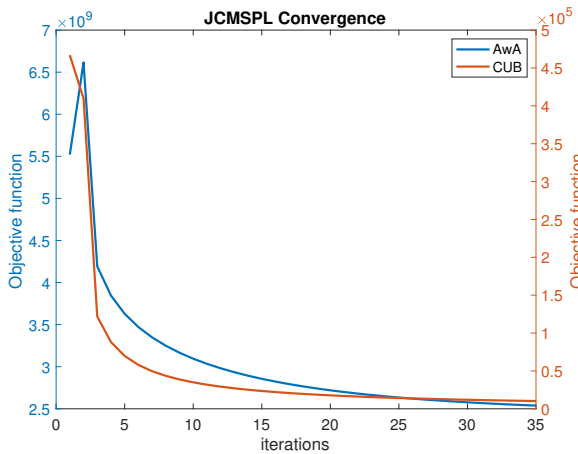


Fig. 5: Convergence of JCMSPL on AwA and CUB Datasets. The left-side vertical axis is for AwA dataset, while the right-side vertical axis is for CUB dataset.

The empirical results also show that our proposed JCMSPL algorithm converges very fast. Figure 5 illustrates the converges curve of JCMSPL on two medium-scale datasets. It is clearly shown that the value of our objective function decreases quickly and stabilize at 35, and our algorithm converges in 35 iterations for all four datasets. Consequently, both of convergence and complexity analysis and empirical

2. The norm $\|\Theta\|$ is any norm which is continuous with respect to the 2-norm of the components, for example their sum of 2-norms.

results all demonstrate that our proposed algorithm JCMSPL is practical to realistic problems by its benefits of good convergence property and low complexity.

5 CONCLUSION

We purposed a novel inductive ZSL method by incorporating the class-specific information in a common latent space and the reconstructions of both visual and semantic features. In contrast to most of the existing ZSL methods, they either do not consider the reconstructions of features nor involve the class-specific information in latent common space. Such class-specific latent space provides more distinct information, and such reconstructions also enhance the robustness by mitigating the domain shifts. Our proposed JCMSPL leverages the instinct structure of visual and semantic features as well as their class-level matching. An efficient algorithm is developed and followed by rigorous theoretic algorithm analysis. Extensive experiments on four benchmark datasets demonstrate that proposed JCMSPL method yields superior classification performances for both standard and generating ZSL than other well-established inductive ZSL methods.

APPENDIX A PROOF CONVERGENCE OF ALGORITHM 1

From the Algorithm 1 in our paper, our primal problem can be written as follows:

$$\begin{aligned} f(\mathbf{A}, \mathbf{B}, \mathbf{C}) = & \frac{1}{2} \|\mathbf{AX}_s - \mathbf{C}\|_F^2 + \frac{\lambda_1}{2} \|\mathbf{BY}_s - \mathbf{C}\|_F^2 \\ & + \frac{\lambda_2}{2} \|\mathbf{C} - \mathbf{H}\|_F^2 + \frac{\lambda_3}{2} \|\mathbf{X}_s - \mathbf{A}^T \mathbf{C}\|_F^2 + \frac{\lambda_4}{2} \|\mathbf{Y}_s - \mathbf{B}^T \mathbf{C}\|_F^2, \end{aligned} \quad (15)$$

And, our algorithm in the paper can also be written as following Algorithm 2 shown in the next page.

Algorithm 2 Joint Concept Matching-Space Projection Learning

At each iteration $t + 1$, compute:

$$\mathbf{A}_{t+1} = \arg \min_{\mathbf{A}} f(\mathbf{A}_t, \mathbf{B}_t, \mathbf{C}_t); \quad (16)$$

$$\mathbf{B}_{t+1} = \arg \min_{\mathbf{B}} f(\mathbf{A}_{t+1}, \mathbf{B}_t, \mathbf{C}_t); \quad (17)$$

$$\mathbf{C}_{t+1} = \arg \min_{\mathbf{C}} f(\mathbf{A}_{t+1}, \mathbf{B}_{t+1}, \mathbf{C}_t); \quad (18)$$

We take $f_t = f(\mathbf{A}_t, \mathbf{B}_t, \mathbf{C}_t)$ for $t = 0, 1, 2, \dots$ and note that the change in L_t can be controlled by the following result:

Theorem 5.

$$\begin{aligned} f_{t+1} - f_t \leq & -\frac{m_A}{2} \|\mathbf{A}_{t+1} - \mathbf{A}_t\|^2 - \frac{m_B}{2} \|\mathbf{B}_{t+1} - \mathbf{B}_t\|^2 \\ & - \frac{m_C}{2} \|\mathbf{C}_{t+1} - \mathbf{C}_t\|^2, \end{aligned} \quad (19)$$

where

$$m_A = \sigma_{\min}(\lambda_3 \mathbf{C}^T \mathbf{C}_t + \mathbf{X}_s^T \mathbf{X}_s) \geq \sigma_{\min}(\mathbf{X}_s^T \mathbf{X}_s) > 0,$$

$$m_B = \sigma_{\min}(\lambda_4 \mathbf{C}_t^T \mathbf{C}_t + \lambda_1 \mathbf{Y}_s^T \mathbf{Y}_s) \geq \sigma_{\min}(\lambda_1 \mathbf{Y}_s^T \mathbf{Y}_s) > 0,$$

$m_C = \sigma_{\min}((1+\lambda_1+\lambda_2)\mathbf{I} + \lambda_3 \mathbf{A}_{t+1} \mathbf{A}_{t+1}^T + \lambda_3 \mathbf{B}_{t+1} \mathbf{B}_{t+1}^T) \geq 1$. The sequence $\{f_t\}_{t=1}^\infty$ is positive and decreasing, hence convergent.

Proof. Respectively denote by $\Delta f_{t,A}, \Delta f_{t,B}, \Delta f_{t,C}$, the change in L corresponding to the update of \mathbf{A} , \mathbf{B} , \mathbf{C} in Eq. (16) - (18). Notice that

$$f_{t+1} - f_t = \Delta f_{t,A} + \Delta f_{t,B} + \Delta f_{t,C}.$$

The function $g(\mathbf{A}) = f(\mathbf{A}, \mathbf{B}_t, \mathbf{C}_t)$ is quadratic and m_A is strongly convex, where m_A is the smallest singular value of Hessian. Hence,

$$\Delta f_{t,A} = g(\mathbf{A}_{t+1}) - \min_{\mathbf{A}} g(\mathbf{A}) \leq -\frac{m_A}{2} \|\mathbf{A}_{t+1} - \mathbf{A}_t\|^2. \quad (20)$$

Similarly, for updating \mathbf{B} and \mathbf{C} , we obtain

$$\Delta f_{t,B} = g(\mathbf{B}_{t+1}) - \min_{\mathbf{B}} g(\mathbf{B}) \leq -\frac{m_B}{2} \|\mathbf{B}_{t+1} - \mathbf{B}_t\|^2, \quad (21)$$

$$\Delta f_{t,C} = g(\mathbf{C}_{t+1}) - \min_{\mathbf{C}} g(\mathbf{C}) \leq -\frac{m_C}{2} \|\mathbf{C}_{t+1} - \mathbf{C}_t\|^2. \quad (22)$$

Summing the inequalities in Eq. (20), Eq. (21), and Eq. (22) then Eq. (19) is proved.

Our primal lost function is as follow

$$\begin{aligned} f_{t,e}(\mathbf{A}, \mathbf{B}, \mathbf{C}) &= \frac{1}{2} \|\mathbf{A}\mathbf{X}_s - \mathbf{C}\|_F^2 + \frac{\lambda_1}{2} \|\mathbf{B}\mathbf{Y}_s - \mathbf{C}\|_F^2 \\ &+ \frac{\lambda_2}{2} \|\mathbf{C} - \mathbf{H}\|_F^2 + \frac{\lambda_3}{2} \|\mathbf{X}_s - \mathbf{A}^T \mathbf{C}\|_F^2 + \frac{\lambda_4}{2} \|\mathbf{Y}_s - \mathbf{B}^T \mathbf{C}\|_F^2, \end{aligned} \quad (23)$$

Hence, we have $f_{t,e} \geq 0$. In particular, we obtain $f_{t+1} = f_{t,e}(\mathbf{A}_{t+1}, \mathbf{B}_{t+1}, \mathbf{C}_{t+1}) \geq 0$. Now, we use complete (strong) indication to show that $f_{t+1} \geq f_t$ for $t = 1, 2, \dots$. Suppose that this holds for $t = 1, 2, \dots, k$. We conclude that $f_t \geq f_1$. Since $m_A > 0$, $m_B > 0$ and $m_C > 1$, according to Eq. (19), we conclude that $f_{t+1} \leq f_t \leq f_1$ which completes the proof. \square

We finally obtain the following corollary which clarifies the statement and gives the proof of our main result in Theorem 4:

Corollary 1. The sequence $\{\Theta_t = (\mathbf{A}_t, \mathbf{B}_t, \mathbf{C}_t)\}_{t=1}^\infty$ satisfies the following:

- a. The parameters for $t = 0, 1, 2, \dots$ are bounded by R , i.e

$$\|\Theta_t\| = \max \{\|\mathbf{A}_t\|, \|\mathbf{B}_t\|, \|\mathbf{C}_t\|\} < R.$$

Hence, the are confined in a compact set.

- b. Any convergence subsequence of $\{\Theta_t\}$ converges to a point $\Theta^* \in U$.
- c. $\text{dist}(\Theta_t, U)$ converges to zero, where

$$\text{dist}(\Theta, U) = \min_{\Theta' \in U} \|\Theta' - \Theta\|$$

Proof. Part a is simply obtained by noticing (23) and the fact that $f_{t,e}(\mathbf{A}_t, \mathbf{B}_t, \mathbf{C}_t) = f_t \leq f_1$, since $\{f_t\}$ is decreasing. For part b, note that since the sequence $\{f_t\}$ is convergent, we have $\lim_{t \rightarrow \infty} f_{t+1} - f_t = 0$, which according to (19) yields

$$\lim_{t \rightarrow \infty} \|\mathbf{A}_{t+1} - \mathbf{A}_t\|_2^2 = \lim_{t \rightarrow \infty} \|\mathbf{B}_{t+1} - \mathbf{B}_t\|_2^2 = \lim_{t \rightarrow \infty} \|\mathbf{C}_{t+1} - \mathbf{C}_t\|_2^2.$$

Moreover, note that the loss function f is f_A -second order Lipschitz with respect to \mathbf{A} (fixing the rest) with $f_A = \|\lambda_3 \mathbf{C}_t^T \mathbf{C}_t + \mathbf{X}_s^T \mathbf{X}_s\|_*$. We obtain that

$$\|\nabla_A f(\mathbf{A}_t, \mathbf{B}_t, \mathbf{C}_t)\|_2^2 \leq f_A^2 \|\mathbf{A}_{t+1} - \mathbf{A}_t\|_2^2$$

which yields

$$\lim_{t \rightarrow \infty} \|\nabla_A f(\mathbf{A}_{t+1} - \mathbf{A}_t)\|_2^2 = 0$$

Similarly, we obtain

$$\lim_{t \rightarrow \infty} \|\nabla_B f(\mathbf{B}_{t+1} - \mathbf{B}_t)\|_2^2 = 0$$

$$\lim_{t \rightarrow \infty} \|\nabla_C f(\mathbf{C}_{t+1} - \mathbf{C}_t)\|_2^2 = 0$$

Now, take a subsequence of $\{\Theta_t\}$ converging to a point $\Theta_* = (\mathbf{A}^*, \mathbf{B}^*, \mathbf{C}^*)$. Since the argument of the above limits are continuous we obtain

$$\nabla_A f(\Theta_*) = 0, \quad \nabla_B f(\Theta_*) = 0, \quad \nabla_C f(\Theta_*) = 0$$

Therefore, $\Theta_* \in U$. For part c, suppose that the claim is not true. Then, according to part a there exists a convergent subsequence of $\{\Theta_t\}$ which is ϵ -distant from U , i.e., $\text{dist}(\Theta_k, U) = \epsilon > 0$. Then, the convergence point is also ϵ -distant from U which contradicts part b and completes the proof. \square

REFERENCES

- [1] O. Russakovsky, J. Deng, H. Su, J. Krause, S. Satheesh, S. Ma, Z. Huang, A. Karpathy, A. Khosla, M. Bernstein *et al.*, "Imagenet large scale visual recognition challenge," *International journal of computer vision*, vol. 115, no. 3, pp. 211–252, 2015.
- [2] P. Sermanet, D. Eigen, X. Zhang, M. Mathieu, R. Fergus, and Y. LeCun, "Overfeat: Integrated recognition, localization and detection using convolutional networks," *arXiv preprint arXiv:1312.6229*, 2013.
- [3] K. Simonyan and A. Zisserman, "Very deep convolutional networks for large-scale image recognition," *arXiv preprint arXiv:1409.1556*, 2014.
- [4] J. Donahue, Y. Jia, O. Vinyals, J. Hoffman, N. Zhang, E. Tzeng, and T. Darrell, "Decaf: A deep convolutional activation feature for generic visual recognition," in *International conference on machine learning*, 2014, pp. 647–655.
- [5] K. He, X. Zhang, S. Ren, and J. Sun, "Deep residual learning for image recognition," in *Proceedings of the IEEE conference on computer vision and pattern recognition*, 2016, pp. 770–778.
- [6] Y. Bengio, A. Courville, and P. Vincent, "Representation learning: A review and new perspectives," *IEEE transactions on pattern analysis and machine intelligence*, vol. 35, no. 8, pp. 1798–1828, 2013.
- [7] R. Socher, M. Ganjoo, C. D. Manning, and A. Ng, "Zero-shot learning through cross-modal transfer," in *Advances in neural information processing systems*, 2013, pp. 935–943.
- [8] C. H. Lampert, H. Nickisch, and S. Harmeling, "Attribute-based classification for zero-shot visual object categorization," *IEEE Transactions on Pattern Analysis and Machine Intelligence*, vol. 36, no. 3, pp. 453–465, 2014.
- [9] L. Fei-Fei, R. Fergus, and P. Perona, "One-shot learning of object categories," *IEEE transactions on pattern analysis and machine intelligence*, vol. 28, no. 4, pp. 594–611, 2006.
- [10] B. M. Lake, R. Salakhutdinov, and J. B. Tenenbaum, "Human-level concept learning through probabilistic program induction," *Science*, vol. 350, no. 6266, pp. 1332–1338, 2015.
- [11] O. Vinyals, C. Blundell, T. Lillicrap, D. Wierstra *et al.*, "Matching networks for one shot learning," in *Advances in neural information processing systems*, 2016, pp. 3630–3638.
- [12] S. Ravi and H. Larochelle, "Optimization as a model for few-shot learning," 2016.

[13] W. J. Scheirer, A. de Rezende Rocha, A. Sapkota, and T. E. Boult, "Toward open set recognition," *IEEE transactions on pattern analysis and machine intelligence*, vol. 35, no. 7, pp. 1757–1772, 2013.

[14] B. Romera-Paredes and P. Torr, "An embarrassingly simple approach to zero-shot learning," in *International Conference on Machine Learning*, 2015, pp. 2152–2161.

[15] Y. Shigeto, I. Suzuki, K. Hara, M. Shimbo, and Y. Matsumoto, "Ridge regression, hubness, and zero-shot learning," in *Joint European Conference on Machine Learning and Knowledge Discovery in Databases*. Springer, 2015, pp. 135–151.

[16] S. Changpinyo, W.-L. Chao, B. Gong, and F. Sha, "Synthesized classifiers for zero-shot learning," in *Proceedings of the IEEE Conference on Computer Vision and Pattern Recognition*, 2016, pp. 5327–5336.

[17] Z. Zhang and V. Saligrama, "Zero-shot recognition via structured prediction," in *European conference on computer vision*. Springer, 2016, pp. 533–548.

[18] W.-L. Chao, S. Changpinyo, B. Gong, and F. Sha, "An empirical study and analysis of generalized zero-shot learning for object recognition in the wild," in *European Conference on Computer Vision*. Springer, 2016, pp. 52–68.

[19] Z. Akata, F. Perronnin, Z. Harchaoui, and C. Schmid, "Label-embedding for image classification," *IEEE transactions on pattern analysis and machine intelligence*, vol. 38, no. 7, pp. 1425–1438, 2016.

[20] Y. Xian, B. Schiele, and Z. Akata, "Zero-shot learning—the good, the bad and the ugly," in *Proceedings of the IEEE Conference on Computer Vision and Pattern Recognition*, 2017, pp. 4582–4591.

[21] P. Kankuekul, A. Kawewong, S. Tangruamsub, and O. Hasegawa, "Online incremental attribute-based zero-shot learning," in *2012 IEEE Conference on Computer Vision and Pattern Recognition*. IEEE, 2012, pp. 3657–3664.

[22] A. Frome, G. S. Corrado, J. Shlens, S. Bengio, J. Dean, T. Mikolov *et al.*, "Devise: A deep visual-semantic embedding model," in *Advances in neural information processing systems*, 2013, pp. 2121–2129.

[23] Y. Fu, T. M. Hospedales, T. Xiang, Z. Fu, and S. Gong, "Transductive multi-view embedding for zero-shot recognition and annotation," in *European Conference on Computer Vision*. Springer, 2014, pp. 584–599.

[24] Z. Akata, S. Reed, D. Walter, H. Lee, and B. Schiele, "Evaluation of output embeddings for fine-grained image classification," in *Proceedings of the IEEE Conference on Computer Vision and Pattern Recognition*, 2015, pp. 2927–2936.

[25] S. Reed, Z. Akata, H. Lee, and B. Schiele, "Learning deep representations of fine-grained visual descriptions," in *Proceedings of the IEEE Conference on Computer Vision and Pattern Recognition*, 2016, pp. 49–58.

[26] J. Lei Ba, K. Swersky, S. Fidler *et al.*, "Predicting deep zero-shot convolutional neural networks using textual descriptions," in *Proceedings of the IEEE International Conference on Computer Vision*, 2015, pp. 4247–4255.

[27] E. Kodirov, T. Xiang, Z. Fu, and S. Gong, "Unsupervised domain adaptation for zero-shot learning," in *Proceedings of the IEEE International Conference on Computer Vision*, 2015, pp. 2452–2460.

[28] S. M. Shoaee and M. S. Baghshah, "Semi-supervised zero-shot learning by a clustering-based approach," *arXiv preprint arXiv:1605.09016*, 2016.

[29] L. Zhang, T. Xiang, and S. Gong, "Learning a deep embedding model for zero-shot learning," in *Proceedings of the IEEE Conference on Computer Vision and Pattern Recognition*, 2017, pp. 2021–2030.

[30] E. Kodirov, T. Xiang, and S. Gong, "Semantic autoencoder for zero-shot learning," in *Proceedings of the IEEE Conference on Computer Vision and Pattern Recognition*, 2017, pp. 3174–3183.

[31] Y. Liu, Q. Gao, J. Li, J. Han, and L. Shao, "Zero shot learning via low-rank embedded semantic autoencoder," in *IJCAI*, 2018, pp. 2490–2496.

[32] Z. Jiang, Z. Lin, and L. S. Davis, "Label consistent k-svd: Learning a discriminative dictionary for recognition," *IEEE transactions on pattern analysis and machine intelligence*, vol. 35, no. 11, pp. 2651–2664, 2013.

[33] W. Tang, A. Panahi, H. Krim, and L. Dai, "Structured analysis dictionary learning for image classification," in *2018 IEEE International Conference on Acoustics, Speech and Signal Processing (ICASSP)*. IEEE, 2018, pp. 2181–2185.

[34] M. Radovanović, A. Nanopoulos, and M. Ivanović, "Hubs in space: Popular nearest neighbors in high-dimensional data," *Journal of Machine Learning Research*, vol. 11, no. Sep, pp. 2487–2531, 2010.

[35] Y. Lu, "Unsupervised learning on neural network outputs: with application in zero-shot learning," *arXiv preprint arXiv:1506.00990*, 2015.

[36] Z. Zhang and V. Saligrama, "Zero-shot learning via joint latent similarity embedding," in *Proceedings of the IEEE Conference on Computer Vision and Pattern Recognition*, 2016, pp. 6034–6042.

[37] M. Rohrbach, S. Ebert, and B. Schiele, "Transfer learning in a transductive setting," in *Advances in neural information processing systems*, 2013, pp. 46–54.

[38] A. Zhao, M. Ding, J. Guan, Z. Lu, T. Xiang, and J.-R. Wen, "Domain-invariant projection learning for zero-shot recognition," in *Advances in Neural Information Processing Systems*, 2018, pp. 1019–1030.

[39] C. Szegedy, W. Liu, Y. Jia, P. Sermanet, S. Reed, D. Anguelov, D. Erhan, V. Vanhoucke, and A. Rabinovich, "Going deeper with convolutions," in *Proceedings of the IEEE conference on computer vision and pattern recognition*, 2015, pp. 1–9.

[40] J. J. Sylvester, "Sur l'équation en matrices $px = xq$," *CR Acad. Sci. Paris*, vol. 99, no. 2, pp. 67–71, 1884.

[41] P. Lancaster and M. Tismenetsky, *The theory of matrices: with applications*. Elsevier, 1985.

[42] R. H. Bartels and G. W. Stewart, "Solution of the matrix equation $ax + xb = c$ [f4]," *Communications of the ACM*, vol. 15, no. 9, pp. 820–826, 1972.

[43] C. Wah, S. Branson, P. Welinder, P. Perona, and S. Belongie, "The caltech-ucsd birds-200-2011 dataset," 2011.

[44] G. Patterson, C. Xu, H. Su, and J. Hays, "The sun attribute database: Beyond categories for deeper scene understanding," *International Journal of Computer Vision*, vol. 108, no. 1-2, pp. 59–81, 2014.

[45] Y. Fu and L. Sigal, "Semi-supervised vocabulary-informed learning," in *Proceedings of the IEEE Conference on Computer Vision and Pattern Recognition*, 2016, pp. 5337–5346.

[46] T. Mikolov, I. Sutskever, K. Chen, G. S. Corrado, and J. Dean, "Distributed representations of words and phrases and their compositionality," in *Advances in neural information processing systems*, 2013, pp. 3111–3119.

[47] Y. Li, D. Wang, H. Hu, Y. Lin, and Y. Zhuang, "Zero-shot recognition using dual visual-semantic mapping paths," in *Proceedings of the IEEE Conference on Computer Vision and Pattern Recognition*, 2017, pp. 3279–3287.

[48] S. Rahman, S. Khan, and F. Porikli, "A unified approach for conventional zero-shot, generalized zero-shot, and few-shot learning," *IEEE Transactions on Image Processing*, vol. 27, no. 11, pp. 5652–5667, 2018.

[49] M. Bucher, S. Herbin, and F. Jurie, "Generating visual representations for zero-shot classification," in *Proceedings of the IEEE International Conference on Computer Vision*, 2017, pp. 2666–2673.

[50] Z. Zhang and V. Saligrama, "Zero-shot learning via semantic similarity embedding," in *Proceedings of the IEEE international conference on computer vision*, 2015, pp. 4166–4174.

[51] M. Norouzi, T. Mikolov, S. Bengio, Y. Singer, J. Shlens, A. Frome, G. S. Corrado, and J. Dean, "Zero-shot learning by convex combination of semantic embeddings," *arXiv preprint arXiv:1312.5650*, 2013.

[52] Z. Fu, T. Xiang, E. Kodirov, and S. Gong, "Zero-shot object recognition by semantic manifold distance," in *Proceedings of the IEEE conference on computer vision and pattern recognition*, 2015, pp. 2635–2644.

[53] A. Mishra, S. Krishna Reddy, A. Mittal, and H. A. Murthy, "A generative model for zero shot learning using conditional variational autoencoders," in *Proceedings of the IEEE Conference on Computer Vision and Pattern Recognition Workshops*, 2018, pp. 2188–2196.

[54] H. Jiang, R. Wang, S. Shan, Y. Yang, and X. Chen, "Learning discriminative latent attributes for zero-shot classification," in *Proceedings of the IEEE International Conference on Computer Vision*, 2017, pp. 4223–4232.

[55] W. Wang, Y. Pu, V. K. Verma, K. Fan, Y. Zhang, C. Chen, P. Rai, and L. Carin, "Zero-shot learning via class-conditioned deep generative models," in *Thirty-Second AAAI Conference on Artificial Intelligence*, 2018.

[56] P. Morgado and N. Vasconcelos, "Semantically consistent regularization for zero-shot recognition," in *Proceedings of the IEEE Conference on Computer Vision and Pattern Recognition*, 2017, pp. 6060–6069.

[57] Z. Ding, M. Shao, and Y. Fu, "Low-rank embedded ensemble semantic dictionary for zero-shot learning," in *Proceedings of the*

IEEE conference on computer vision and pattern recognition, 2017, pp. 2050–2058.

- [58] Y. Xian, T. Lorenz, B. Schiele, and Z. Akata, “Feature generating networks for zero-shot learning,” in *Proceedings of the IEEE conference on computer vision and pattern recognition*, 2018, pp. 5542–5551.
- [59] S. Kolouri, M. Rostami, Y. Owechko, and K. Kim, “Joint dictionaries for zero-shot learning,” in *Thirty-Second AAAI Conference on Artificial Intelligence*, 2018.
- [60] H. Chen, L. Cao, and R. Ji, “Learning similarity-specific dictionary for zero-shot fine-grained recognition,” in *ICASSP 2019-2019 IEEE International Conference on Acoustics, Speech and Signal Processing (ICASSP)*. IEEE, 2019, pp. 3697–3701.
- [61] F. Shen, X. Zhou, J. Yu, Y. Yang, L. Liu, and H. T. Shen, “Scalable zero-shot learning via binary visual-semantic embeddings,” *IEEE Transactions on Image Processing*, 2019.